β-delayed neutron decay of ^{14}Be

M. D. Belbot, J. J. Kolata, K. Lamkin, R. J. Tighe,* and M. Zahar
Physics Department, University of Notre Dame, Notre Dame, Indiana 46556

R. Harkewicz,† D. J. Morrissey, N. A. Orr,‡ R. M. Ronningen, B. M. Sherrill, and J. A. Winger§
Cyclotron Laboratory, Michigan State University, East Lansing, Michigan 48824

M. Carpenter
Physics Division, Argonne National Laboratory, Argonne, Illinois 60439
(Received 23 November 1994)

The neutron spectroscopy of the β-delayed neutron decay of ^{14}Be has been investigated. Two neutron groups were observed, and energy limits are given for a third (unobserved) group that receives most of the β-decay strength. Branching ratios and logft values deduced for all three groups are compared with the results of a shell-model calculation.

PACS number(s): 23.40.Hc, 27.20.+n

I. INTRODUCTION

The neutron drip-line isotope ^{14}Be is of considerable interest since it is believed to have "neutron halo" structure as revealed by total interaction cross section [1] and momentum distribution [2] measurements. It is known that ^{14}Be is a β-delayed one- and two-neutron emitter [3]; the branching ratios for these decay modes have been measured by Dufour *et al.* [4], who obtained $10 \pm 3\%$ for $0n$ decay, $81 \pm 4\%$ for $1n$ decay, and $5 \pm 2\%$ for $2n$ decay. Nothing is known about the population of individual final states in the daughter nucleus ^{14}B, and its level scheme is poorly known. Theoretical work has been done in this area, however. A shell-model calculation by Curtin and Brown [5] predicts a 98% β-decay branch to a state that is just below the single neutron emission threshold and a weak (0.5%) branch to an excited state of ^{14}B just above the single-neutron threshold. The remaining strength appears as even smaller branches to other levels. This calculation therefore is in sharp disagreement with the measured branching ratios for neutron decay given above. This large discrepancy motivated us to perform a detailed neutron spectroscopy measurement for the decay of ^{14}Be.

II. EXPERIMENTAL METHOD

The experiment was performed at the National Superconducting Cyclotron Laboratory (NSCL) at Michigan State University (MSU). Due to the short half-life [4] of ^{14}Be (4.35 ± 0.17 ms), an implanted radioactive beam was used to carry out the β-decay study. The primary beam for this experiment was 80 MeV per nucleon ^{18}O ions produced by the K1200 cyclotron, which impinged on a ^{9}Be target having a thickness of 790 mg/cm^2. The ^{14}Be fragments were collected and separated using the A1200 fragment mass separator [6]. For this experiment, the first section of the A1200 was set to select fragments with a mass-to-charge ratio of 3.5. An aluminum degrader wedge having a central thickness of 425 mg/cm^2 and an angle of 3.5 mrad (the degrader configuration corresponding to achromatic separation [7]), located at the second dispersive image, allowed for further purification of the secondary beam. The ^{14}Be beam had an intensity of 110 particles per second with an average energy of 61.17 MeV per nucleon. It was transported to a low background experimental vault 30 m away from the fragment separator where the measurements were performed.

The beam was stopped inside a 2.0 cm by 2.5 cm piece of BC412 plastic scintillator that was 1 cm deep. This provided the "start" signal that indicated the β decay of the implanted nuclei. An 8 mm aluminum energy degrader was introduced between the 0.25 mm Kapton beam entrance window and the implantation detector to adjust the implantation depth of ^{14}Be ions. The distance to which the ^{14}Be beam penetrated into the scintillator, determined by the initial beam energy and the density and composition of the various absorbers, was 0.72 ± 0.05 cm (including energy straggling and the 6% energy spread in the incident beam).

A thin (ΔE) Si surface barrier detector of thickness 0.2 mm and area 300 mm^2 was placed in front of the implantation detector to monitor the purity of the beam. A plot of the energy loss in the ΔE detector versus the timing signal (TOF$_{rf}$) from a scintillator at the first dispersive image of the A1200, relative to the cyclotron RF, yields clear Z and A separation (Fig. 1). A similar plot gated in coincidence with an E-veto detector placed behind the implantation detector yielded the number and

*Present address: Bldg. 88, Lawrence Berkeley Laboratory, Berkeley, CA 94720.
†Present address: Physics Division, Argonne National Laboratory, Argonne, IL 60439.
‡Present address: LPC-ISMRA, Boulevard du Marechal Juin, 14050 Caen Cedex, France.
§Present address: Dept. of Physics, Mississippi State University, Mississippi State, MS 39762.

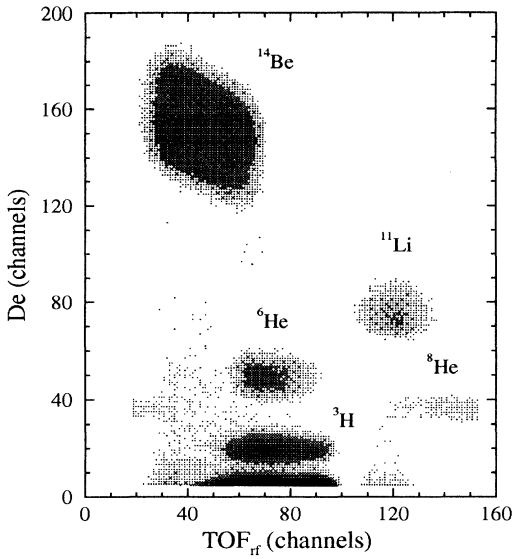

FIG. 1. Plot of energy loss in the ΔE detector versus timing signal referenced to the cyclotron RF (TOF$_{rf}$).

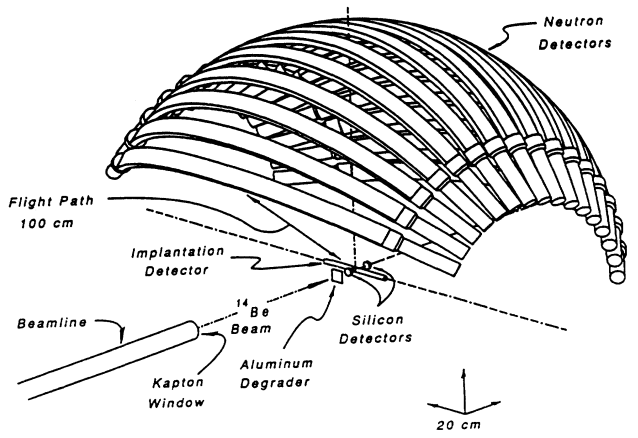

FIG. 2. Schematic diagram of the neutron detector array and experimental setup [8].

species of particles that passed through this detector, and therefore were not implanted. The purity of the secondary beam stopped in the implantation detector was $90 \pm 4\%$. A summary of the beam composition is given in Table I.

The cyclotron was cycled on and off at periodic intervals by dephasing one of its "dees" to enable measurement of the β decay with no interference from direct beam. For this experiment two different duty cycles were used: 10.3 ms on followed by 10.3 ms off and 10.3 ms on followed by 40.0 ms off. The first duty cycle yielded higher statistics, while the contribution from the daughter decays was better estimated with the second cycle.

The neutrons were detected in an array of 15 rectangular plastic scintillators (BC412) 157 cm by 7.6 cm by 2.54 cm thick that are bent in a 1 m radius of curvature (see Fig. 2 and Ref. [8]). This ensures that the neutron flight path is constant within a few millimeters. The total solid angle of the detector array is approximately 1.8 sr. The scintillator material is sensitive not only to neutrons but also to electrons and γ rays. Since the neutrons are much slower than the prompt electrons and γ rays produced in the decay of ^{14}Be, they were easily isolated.

TABLE I. Total percentages of the various components of the beam stopped in the implantation detector (see text).

Isotope	Yield (%)
^{14}Be	90±4
^{11}Li	3.7±0.1
^{8}He	1.2±0.3
^{6}He	1.2±0.1
^{3}H	3.7±0.1

Scattered electrons and γ rays cannot be distinguished, and these contribute to the background.

A high-purity Ge detector was used to measure the γ-ray transitions that might be coincident with the neutron decays, to construct fully the decay scheme of ^{14}Be. This detector was placed so that it did not block the beam, nor the view of the implantation detector by the neutron detectors. It had a resolution of 1.97 keV (FWHM) and an efficiency 88.4% of that of NaI at 1.33 MeV. The crystal was 75.8 mm in diameter and 92.9 mm in length and was placed with its front face 83 ± 3 mm away from the center of the implantation detector.

A calibration of the neutron detector with a ^{17}N beam was taken at the end of the experiment. This isotope has four neutron peaks with well-known energies and branching ratios [9], two of which (1.7003 and 1.1709 MeV) were suitable for determining the neutron detection efficiencies and to accurately measure the neutron flight path. A Pu-Be source was used to extend the efficiency measurements to higher energies. Useful statistics were obtained for 1.4 to 7.3 MeV neutrons.

III. RESULTS

The β-decay curve is found by measuring the time difference between the start of the beam-off period and an event in the implantation detector during the same beam-off period. The fit to the ungated (raw) β-decay curve for ^{14}Be (Fig. 3) was complicated by the presence of impurities and contributions from the decay of the daughters. The beam-off period (10 or 40 ms) is of the same order of magnitude as the half-lives of the daughters (approximately 20 ms), and therefore there will be a buildup of daughters to a saturation value after several beam cycles. Also, the amount of the daughter present increases for a short time after the beam is turned off because of the decay of the parent. A computer program was written to model the growth and decay of ^{14}Be, its daughters,

and the impurities for each beam-on/off cycle. The average β-decay end-point energies of ^{14}Be and its daughters (weighted by the branching ratios and Q values for decay to daughter states) range from 13.9 to 16.2 MeV. Since the average β-decay energy is one-third of the end-point energy, the average electron energy for the present experiment ranges from 4.5 to 5.4 MeV, and thus the electrons are minimum ionizing. The energy loss of the electrons from the β decay of ^{14}Be and its daughters in BC-412 plastic should therefore be very similar, differing by only 2% [10]. Because the energy loss for the β decay of ^{14}Be and its daughters is roughly equal to that of minimum ionizing electrons (0.51 MeV[10] at a β energy of about 2 MeV) and is much greater than the threshold energy of the implantation detector indicated by its high β-detection efficiency (see below), the β-detection efficiencies are nearly identical. Since the impurities are not implanted at the same depth into the plastic, their β-detection efficiencies cannot *a priori* be assumed to be the same as that of ^{14}Be, but (as shown below) the impurity levels were found to be negligibly small (well within systematic error) in the fit of the raw β-decay curve. Therefore the β-detection efficiencies for all nuclei (parent, daughters, and impurities) were assumed to be the same. The data with the longer beam-off period (40 ms) was used for the fit to the raw β-decay curve. This period is approximately equal to 10 half-lives of the parent, when only 0.1% of the initial activity is still present. Because two of the impurities, ^{6}He and ^{3}H, have very long half-lives (806.7 ms [11] and 12.3 yr [12], respectively), they were treated as part of a constant background for the purposes of the fit. The background was determined by fitting the last 9.3 ms of the decay curve with a two-component exponential and a constant background having half-lives fixed to that of ^{14}B and ^{13}B (13.8 ± 1.0 ms and 17.36 ± 0.16 ms, respectively) [3]. The relative abundances of the daughters were calculated from the branching ratios determined by Dufour *et al.* [4] and were held fixed for the purposes of the fit. The branching ratio to ^{12}B is too small ($5 \pm 2\%$) [4] to be fit accurately, but even complete exclusion of this component did not significantly alter the results. The implantation rate of ^{14}Be and its half-life were then varied to minimize the reduced χ^2 of the fit, giving a half-life equal to $4.8 \pm 0.4 \pm 0.2$ ms (everywhere the first uncertainty is statistical and the second systematic) with reduced $\chi^2 = 0.98$ and a detected implantation rate of 0.0604 ± 0.0005 ^{14}Be ions per ms. The error in estimating the constant background contributed the majority of the systematic error. Another fit to the β-decay curve was done using the program LIFE5 [13], which fits a constant background and radioactive daughters, but no impurities. The impurities. The impurities are very small and do not change the fit appreciably: the total abundance of the parent differed by only 1.8%, and the half-life by 3.1%, between the two programs. The fit to the raw β-decay curve including the parent, daughters, impurity, and background yields is shown in Fig. 3 and resulted in a total measured ^{14}Be yield of $(2.04 \pm 0.01 \pm 0.24) \times 10^6$. Thus the systematic error in the ^{14}Be yield (12%) is much greater than the difference between the results of two programs

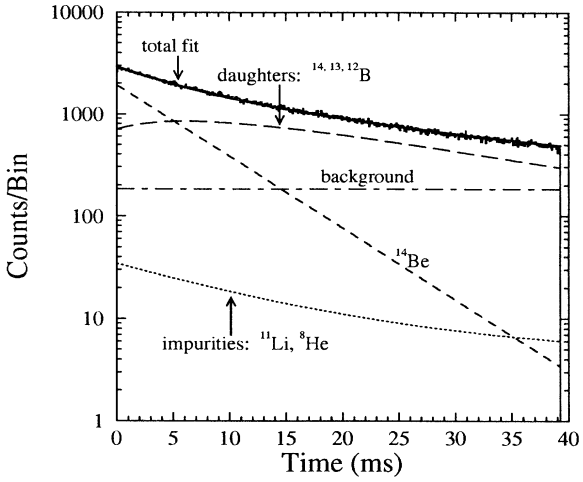

FIG. 3. Fit of the raw β-decay curve for ^{14}Be showing ^{14}Be, daughter, impurity, and background components.

given above (1.8%). The decay curve requiring β-n coincidence was also fit with a single exponential and a constant background using LIFE5. The resulting half-life was 4.0 ± 1.2 ms, and the fit (shown in Fig. 4) had a reduced $\chi^2 = 1.7$.

The intrinsic (not including solid angle) neutron detection efficiency as a function of energy must be found to obtain the branching ratios for neutron emission. The data points shown in Fig. 5(a) came from three sources. First, the efficiency for the 1.1709 MeV and 1.7003 MeV peaks of ^{17}N were obtained in this work from the known branching ratios [9]. Second, the efficiency for the 0.810 and 1.714 MeV groups from β-delayed neutron decay of ^{16}C was obtained by reanalysis of the data of Scheller *et al.* [13] who used the same neutron detector array and

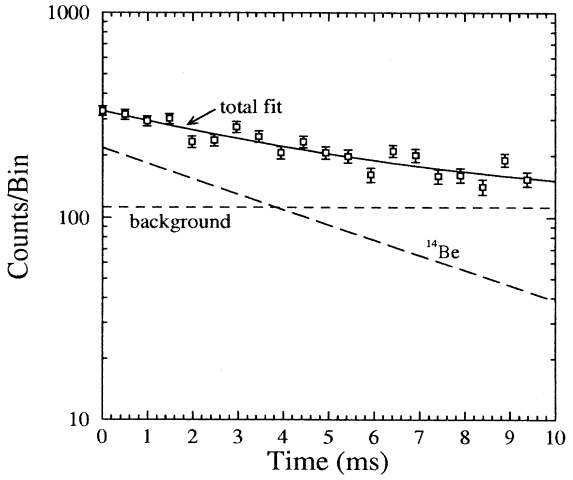

FIG. 4. Fit of the decay curve obtained by requiring β-n coincidence.

discriminator settings as the present experiment. (The efficiency of the 1.1709 MeV and 1.7003 MeV ^{17}N peaks were also determined in Ref. [13].) Last, the efficiencies for 1.7, 2.2, 2.8, 3.4, 4.0, and 4.6 MeV neutrons from the Pu-Be source have been determined in this work by direction comparison to the count rate found in a small cylindrical neutron detector (BC 501, radius 3.375 cm and depth 3.6 cm). Its front face was 97.4 ± 0.6 cm from the center of the implantation detector (solid angle 3.77 ± 0.06 msr).

The intrinsic neutron detection efficiencies could be reliably calculated to within 10% using the Monte Carlo code KSUEFF [14] that is based on a program [15] of Kurz. The Pu-Be measurement agreed within mutual errors with the ^{17}N efficiency determination at 1.7 MeV. The efficiencies for the ^{17}N peaks were obtained by fitting the β-decay curve to obtain the total number of β decays.

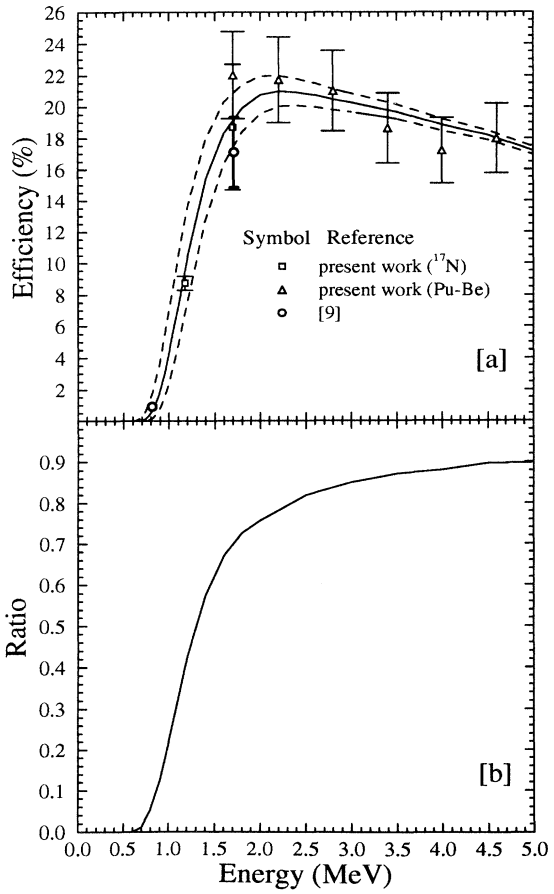

FIG. 5. (a) The solid line represents the best fit to the data of the present work and Ref. [13] using the Monte Carlo program KSUEFF (see text and Ref. [14]). The dashed lines represent the systematic error in the neutron efficiency due to the uncertainty in the threshold of the neutron detectors (also calculated using KSUEFF). (b) Semilog plot of the ratio of the neutron efficiency of the present work to that of Ref. [17], both calculated using KSUEFF.

Since the ^{17}N beam was 100% pure and ^{17}N produces the stable daughter ^{17}O, the β-decay curve could be fit with a single exponential and a constant background. Then, the time-of-flight spectrum was used to determine the total number of neutrons detected for each peak. The expected number of neutrons, and hence the intrinsic neutron detection efficiency, was determined from the number of β decays and the known branching ratios. Note that it was not necessary to correct for β-detection efficiency, since the time-of-flight spectrum is gated on the implantation detector and therefore the same β-detection efficiency is folded into both the half-life and time-of-flight spectra. A plot of neutron efficiency as a function of energy is shown in Fig. 5(a). One obtains a threshold for neutron detection equal to 0.77 ± 0.13 MeV by extrapolating this curve to zero efficiency. This threshold (expressed as electron equivalent energy) is an input parameter to KSUEFF [14] which was run for various thresholds. The calculation that best matched the data had a threshold of 0.16 MeV electron equivalent energy and is shown as a solid line in Fig. 5(a). The two dashed curves represent the estimate of the uncertainty in this threshold (± 0.02 MeV), which is a systematic error in the efficiency calculation.

The branching ratios for ^{14}Be can now be determined using the above neutron efficiency curve. We discovered that there was a small amount of beam-on contamination in the data. Even though the cyclotron is turned off at the end of the bombardment phase, the beam must still traverse about 30 m of beam line, which results in some beam being present at the beginning of the counting cycle. This problem is remedied by excluding the time-of-flight events associated with the first 0.110 ms of the beam-off period, and correcting the decay curve to its true beginning. Figure 6 shows a neutron time-of-flight spectrum for the sum of all 15 detectors. The average energy for β decay to the ground state of ^{14}B (equal to one-third of the end-point energy) is 5.40 ± 0.04 MeV;

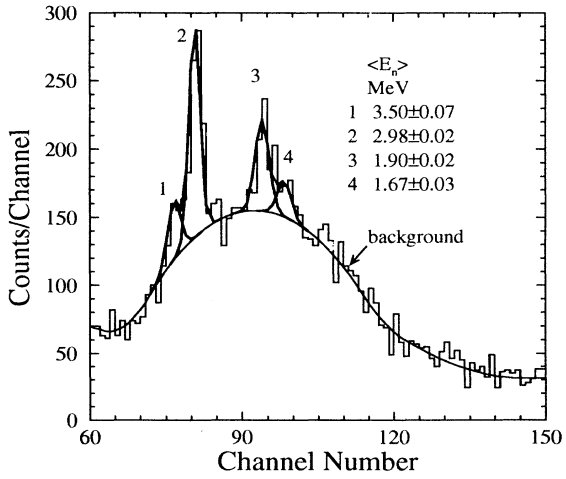

FIG. 6. Raw time-of-flight spectrum giving the sum of the data from all 15 detectors in the array. The bold lines indicate fits to individual peaks.

consequently the velocity of the electrons is essentially that of light. These highly relativistic electrons conveniently serve as a "time zero" marker when corrected for their flight time. The four neutron peaks shown in Fig. 6 were fitted simultaneously, with Gaussian line shapes and a cubic polynomial background, using the computer program FITS [16].

In a recent experiment at MSU, Morrissey *et al.* measured the β-delayed neutrons from the decay of ^{11}Li using the same neutron detector array as the present experiment [17]. Two of the neutron groups observed in this experiment (3.50 and 1.90 MeV) have energies consistent (within experimental error) with the ^{11}Li delayed neutron energies given in Table II. This suggests that there is ^{11}Li contamination in the data, as was apparent in Fig. 1. We discovered that one of the peaks in Fig. 6, at 1.90 MeV, comes entirely from ^{11}Li. The decay curve for this peak (Fig. 7) yields a half-life of 7.5 ± 0.9 ms, which is consistent (within error) with the accepted half-life [18] of ^{11}Li (8.5 ± 0.2 ms). In this plot, the background has been subtracted from the ^{14}Be decay curve by gating on two regions of the time-of-flight spectrum (channels 85–88 and 102–106) which contained only background counts, thereby obtaining the background decay curve. The total number of counts in both regions equaled the number of counts above background in the 1.90 MeV peak, so that the "background" decay curve could be subtracted directly from the data. Because this neutron transition comes entirely from ^{11}Li, the ^{11}Li spectrum could be normalized to the corresponding peak in the data. Since the threshold for the experiment of Ref. [17] was 350 keV, whereas in the present experiment it was 770 keV, a correction must be made for the difference in neutron efficiency. The ^{11}Li data were corrected for the difference in efficiency of both experiments by multiplying, channel by channel, the time-of-flight spectrum by the efficiency of the present experiment divided by that of the ^{11}Li experiment (which was also found using KSUEFF [14]). Since the same detector array was used, no correction for solid angle was required. Then, the resulting time-of-flight spectrum was subtracted from the raw ^{14}Be time-of-flight spectrum, and the ^{11}Li contamination was thereby removed. The ratio of the two calculated efficiency curves is shown in Fig. 5(b). The total percentage of ^{11}Li contamination calculated from the data of Ref. [17] was $2.9 \pm 0.9\%$, whereas $3.7 \pm 0.1\%$ was obtained from the direct impurity measurement in the present experiment (see Fig. 1 and Table I).

The time-of-flight plot with the ^{11}Li contamination removed is shown in Fig. 8. The two remaining sharp peaks shown were fitted simultaneously with a cubic background and Gaussian line shapes using FITS. These likely represent single-neutron decay or possibly sequential $2n$ decay through narrow intermediate states. Direct two-neutron decay to the continuum, by contrast, is a three-body decay process and thus does not give neutrons of unique energies. The polynomial background mainly results from such direct $2n$ decay, or possibly but less likely from neutron decay to broad, closely spaced final $1n$ states. This point will be discussed further below. The true background was fit separately and consisted of two parts: a constant level that represents random coincidences, and an increasing component (also a cubic polynomial) on the high-energy (short time-of-flight) side representing the long tail of the β peak resulting from late-arriving scattered electrons or photons as discussed above. The energies for the narrow neutron groups were deduced from the centroids given in Fig. 8. Since the width of the higher energy peak was rather ill defined and the calculated experimental widths (about 2.5 and 2.6 channels for the 3.52 and 3.02 MeV peaks, respectively) only differ by 5%, the width of the 3.52 MeV peak was held fixed relative to that of the 3.02 MeV peak. The resulting common width for both peaks was 2.3 channels, differing from the calculated widths by 12% at most.

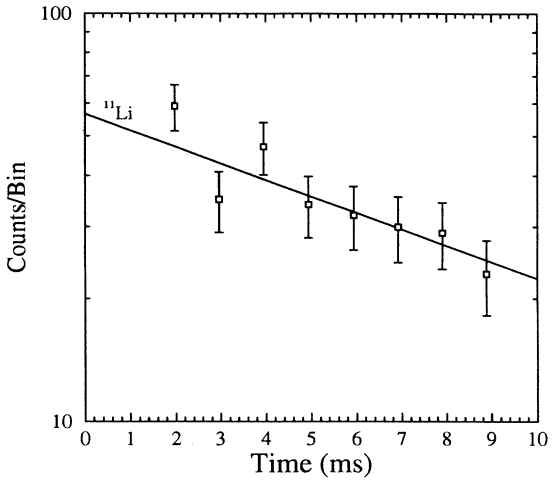

FIG. 7. Fit of the ^{11}Li decay curve after background subtraction.

TABLE II. Energies and widths of β-delayed neutron groups from ^{11}Li (Ref. [17]).

Peak No.	$\langle E_n \rangle$ (MeV)	σ (keV)
1	6.11	612
2	3.48	186
3	2.91	115
4	1.88	118
5	1.51	468

We did not use Fig. 1 (ΔE versus $\mathrm{TOF_{rf}}$) to determine the total number of detected β decays because this introduces an additional systematic error that is unnecessary since this number can be determined directly from the raw β-decay curve. The β-detection efficiency for ^{14}Be decays was found by calculating the activity at the end of the beam-on period and dividing this by the activity measured by the implantation detector at the beginning of the beam-off period (Fig. 3). The implantation rate R is calculated by dividing the number of ^{14}Be ions implanted (found from the ΔE and E veto data) by the total beam-on time (the number of cycles times the

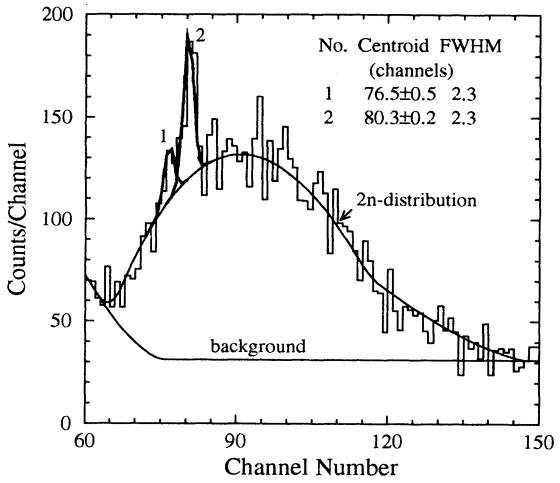

FIG. 8. Time-of-flight spectrum for the sum of all 15 neutron detectors with ^{11}Li contamination removed. This spectrum has not been corrected for neutron detection efficiency. The bold lines indicate fits to individual peaks; the Arabic numerals refer to peaks listed in Table IV.

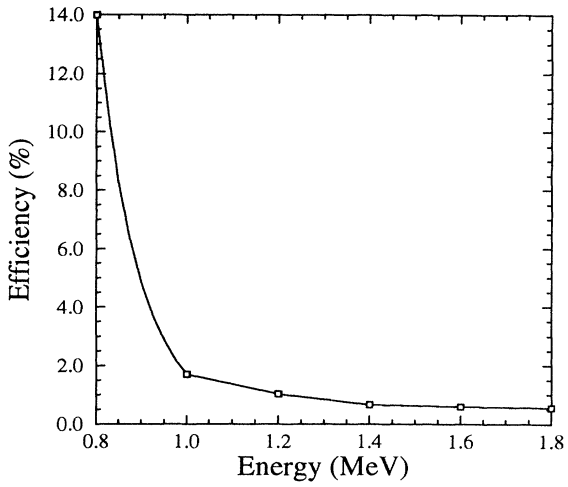

FIG. 9. The two-standard-deviation upper limit of the branching ratio to a hypothetical unobserved neutron state, plotted as a function of neutron energy. The points represent calculations at various neutron energies, and the curve is a cubic spline interpolation.

beam-on period). The activity at the end of the beam-on period, A, is given by $A = R(1 - e^{-\lambda t})$, where λ is the decay constant for ^{14}Be (where the accepted half-life, 4.35 ± 0.17 ms,[14] was used) and t is the beam-on period (10.3 ms). For the long duty cycle runs, the β detection efficiency was $80 \pm 10\%$. Assuming that the center of the implanted activity is 0.72 cm away from the center of the front face of the implantation detector (2.0 cm by 2.5 cm by 1.0 cm deep), the minimum distance (on average) through which the β particles traverse before exiting is 0.28 cm. The energy loss for electrons with an average β decay energy (4.4–5.4 MeV in the present experiment) traveling through this distance of scintillator plastic is about 0.6 MeV [10], which is much larger than the threshold of the implantation detector. Thus one would expect the β detection efficiency to be quite high as observed. The branching ratios, given in Table III, were calculated by normalizing the neutron yields for neutron detection efficiency and solid angle, and dividing by the total number of β decays measured by the implantation detector ($[2.04 \pm 0.01 \pm 0.24] \times 10^6$) determined from the ^{14}Be component of the fit to the raw β decay curve (Fig. 3).

In the present experiment, it is important to determine what was not observed. In particular, upper limits were determined for the strength of an unobserved neutron peak with an energy below that of the lowest observed peak. In Fig. 9 the two-standard-deviation upper limit for the branching ratio to a hypothetical unobserved neutron emitting state is plotted as a function of neutron energy. This result will be used below to estimate the branching ratio to a suggested state below the threshold of the neutron detectors in this experiment.

The only γ-ray transitions found corresponding to the daughters of ^{14}Be were the ground-state decays of the known 3.5346 MeV and 3.6810 MeV levels in ^{13}B [3]. The measured energies were 3.528 ± 0.001 MeV and 3.680 ± 0.001 MeV, respectively. Unfortunately, due to poor statistics, no useful information could be derived from the γ-n coincidence data. However, it was possible to estimate the branching ratios (relative to the total number of β decays) and place limits on the logft values for the population of the two ^{13}B excited states. The intrinsic efficiency of the γ-ray detector was measured by using a calibrated National Institute of Standards and Technology point source (a mixture of ^{125}Sb, ^{154}Eu, and ^{155}Eu) for which the absolute γ emission rates had been

TABLE III. Logft values for the β decay of ^{14}Be, assuming $1n$ emission to different final states in ^{13}B. (The energies of the final levels are given in parentheses.) Under the headings Branching ratio and Logft, the first uncertainties listed are statistical, and the second are systematic.

No.	Energy (MeV)	Branching ratio (%)	Logft (g.s.)	Logft (3.5346 MeV)	Logft (3.6810 MeV)
1	3.52±0.07	0.11±0.02±0.04	$6.00\pm^{0.06}_{0.07}\pm^{0.14}_{0.20}$	$5.24\pm^{0.07}_{0.08}\pm^{0.14}_{0.20}$	$5.20\pm^{0.07}_{0.08}\pm^{0.14}_{0.20}$
2	3.02±0.03	0.30±0.03±0.05	$5.67\pm^{0.05}_{0.05}\pm^{0.07}_{0.09}$	$4.95\pm^{0.05}_{0.06}\pm^{0.08}_{0.09}$	$4.91\pm^{0.05}_{0.06}\pm^{0.08}_{0.09}$

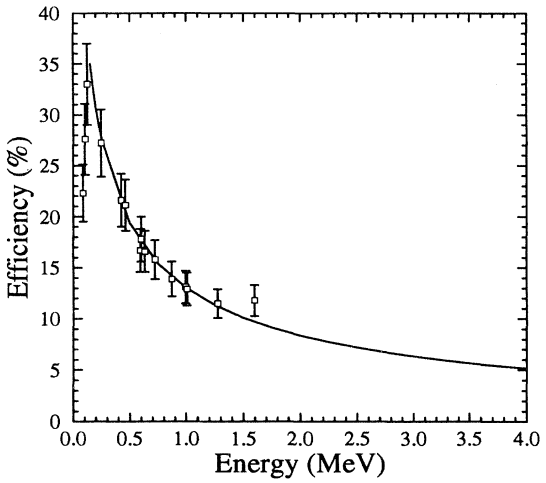

FIG. 10. Intrinsic efficiency for the high-purity Ge detector used in this work. The data points represent the measured efficiency for the strongest lines of the calibration source and the solid line represents the best fit to the data (see text).

determined to within 1.3% for the strongest lines [19]. Because the source was placed off axis (by 22 ± 3 mm), the Monte Carlo code of Wieloposki [20] was used to calculate the solid angle of the Ge detector (0.51 ± 0.05 sr) assuming an isotropic point source. A correction for the dead time, which was about 68.7%, was also applied. The plot of the intrinsic efficiency as a function of γ-ray energy shown in Fig. 10 (extended to 4 MeV) has been fitted to the function [21]:

$$\ln \varepsilon = bx + cx^2; x = \ln(a/E) \ ,$$

where ε is the efficiency in percent, E is the γ-ray energy in keV, and a, b, and c are constants. The best fit yielded $a = 2.8 \times 10^{-5}$, $b = -0.9063$, and $c = -0.04349$. The code of Wieloposki [20] was also used to calculate the solid angle of the γ-ray detector as seen by the implantation detector (0.57 ± 0.05 sr, slightly larger than that above since it is on axis). The intrinsic efficiencies for the 3.5346 and 3.6810 MeV transitions of ^{13}B were $5.9 \pm 0.6\%$ and $5.7 \pm 0.5\%$, respectively (Fig. 10), and the branching ratios were approximately 0.6% and 2.7%, respectively. Assuming that a single state of ^{14}B below the $2n$-threshold (5.85 MeV) populates the observed states of ^{13}B, the possible ranges of logft values using the method of Wilkinson and Macefield [22] (see below) were 4.9–5.6 (3.5346 MeV) and 4.3–4.7 (3.6810 MeV). These branching ratios and logft values are only rough estimates, of course, because the effects of the distribution of implanted ^{14}Be ions, pile-up events, and the systematic error in the extension of the efficiency curve have not been considered.

IV. DISCUSSION

The half-life for ^{14}B β decay obtained from the raw β decay curve ($4.8 \pm 0.2 \pm 0.4$ ms) agrees (within error) with the value of 4.0 ± 1.2 ms obtained from β-n coincidence data, and both agree within experimental error with the accepted value of 4.35 ± 0.17 ms. The coincidence data have limited statistics, and the raw decay curve half-life has a rather large systematic uncertainty because the daughter activities have half-lives similar to that of ^{14}Be. We therefore use the accepted half-life (4.35 ± 0.17 ms)[4] to compute logft values, where

$$\log(ft) = \log_{10}\left[\frac{f(Z,E_0)T_{1/2}}{\text{B. R.}}\right] \ ,$$

and B. R. is the branching ratio for the state in question. The Fermi integral $f(Z,E_0)$ for an allowed decay was computed using the method of Wilkinson and Macefield [22]. The Q value for decay to the ^{14}B ground state is 16.21 ± 0.11 MeV [23], the neutron separation energy is 0.97 MeV, and the nuclear recoil energy of the daughter is already accounted for in this method. The computation of $f(Z,E_0)$ is parametrized in the form

$$f(Z,E_0) = f_{(Z=0)} \exp\left[\sum_{n=0}^{3} a_n (\ln E_0)^n\right] \ ,$$

where a_n are the coefficients given in Table IV and $f_{(Z=0)}$ is the point nuclear phase space factor for $Z = 0$ (see Ref. [22]). The logft values for the two observed neutron groups are given in the fourth column of Table III, under the assumption that they decay to the ground state of ^{13}B. Each of these is consistent with an allowed Gamow-Teller transition to a 1^+ state in ^{14}B. Other possibilities cannot be excluded, however. First, the observation of γ decay from the 3.5346 and 3.6810 MeV states in ^{13}B suggests the possibility that some of these neutron groups may correspond to decays to these states. It was not possible to obtain γ-n coincidence data, and therefore the final state could not be uniquely determined. However, it is unlikely that the two observed neutron groups

TABLE IV. The coefficients a_n used to calculate logft values in this work (see text and Ref. [22]).

Coefficient	β End-point energy range (MeV)		
	0.501–3.162	3.163–13.589	12.590–25.044
a_n	0.172 856	−0.049 740 9	0.015 828 4
a_1	0.155 095	−0.016 688 5	0.0
a_2	0.109 009	−0.099 452 3	−0.023 468 4

populate excited states in ^{13}B, since that would place the excitation energy of the corresponding states in ^{14}B well above the $2n$-decay threshold (5.85 MeV). The logft values for the two neutron groups are given in Table III under the assumption that they decay to states in ^{13}B; all are consistent with allowed transitions. Another possibility has already been alluded to above: without coincidence data, we cannot rule out the possibility that some of the neutron groups come from sequential $2n$ emission through narrow excited states in ^{13}B. In particular, the decay energy for the neutron decay of the known state in ^{13}B at 8.683 MeV[3] to the ground state of ^{12}B corresponds, within experimental error, to the neutron group at 3.52 ± 0.07 MeV. The maximum β-decay end-point energy for this transition would be 6.67 MeV, assuming the coincident neutron had essentially zero energy. The maximum logft value of 5.1 corresponding to such a state would imply an allowed transition.

We next turn our attention to the broad neutron distribution underlying the narrow peaks, much of which likely corresponds to the $2n$-decay channel. From the fit to this distribution given in Fig. 8 and the neutron efficiency curve in Fig. 5(a), we deduce a $2n$ branching ratio of $5 \pm 1 \pm 2\%$ for neutrons above 0.83 MeV, where the systematic error includes the uncertainty in the efficiency curve that is large near threshold. (Note that the measured fraction of neutrons in the broad group has been divided by two to account for the fact that either of the two neutrons can be detected.) In determining the $2n$ branching ratio, we excluded the region from 0.83 MeV to threshold (0.77 MeV) since the efficiency in this region is ill defined. The calculated branching ratio in the present work is consistent with that obtained by Dufour *et al.* [4] assuming that all of the broad distribution corresponds to β-delayed $2n$ emission, and little of it is below the threshold of the neutron detectors. However, scattered photons and electrons will induce an energy-dependent background [8] under the broad group that is difficult to determine and has been ignored above. The sum of the branching ratios for the two observed $1n$ states is $0.41 \pm 0.03 \pm 0.07\%$. Therefore the total observed neutron branching ratio is at most about 7% (including systematic error), compared with the 86% expected when account is taken of the 14% $0n$ branch (Ref. [4]). Consequently, 77–85% (including systematic errors) of the neutron yield is missing. We suggest that most of this missing yield results from $1n$ decay to a state in ^{14}B with an excitation energy between 0.97 and 1.80 MeV, such that the corresponding neutron group is below the threshold of our neutron detectors. Also some of the missing yield could result from higher-energy $1n$ emitting states of ^{14}B corresponding to the 3.5346 MeV and 3.6810 MeV γ-ray transitions observed in ^{13}B as described above. These neutron emitting states of ^{14}B cannot be uniquely determined (due to lack of γ-n coincidence data) and were not included above. However, they are rather minor in importance in explaining the missing yield because the sum of the branching ratios for the two states is 3.3%, whereas the missing yield has a branching ratio of 80%.

The known [3] states of ^{14}B and the thresholds for one- and two-neutron decay are illustrated in Fig. 11 together

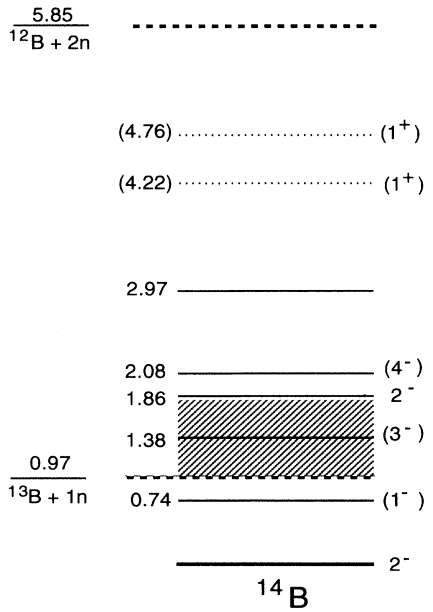

FIG. 11. Level diagram of states in ^{14}B (energies in MeV). The dotted lines represent states determined in the present experiment, under the assumption that the neutron groups all correspond to decays to the ground state of ^{13}B (see text for a discussion of other possibilities). The shading indicates the energy region in which an inferred but unobserved neutron emitting state must lie.

with the new states determined in the present work under the assumption that all neutron groups correspond to transitions to the ground state of ^{13}B. The shaded region represents the possible energy range for the state that accounts for the missing neutrons as described above. Depending on the actual excitation energy and branching ratio of this state, the corresponding logft value lies between 3.6 and 3.8, implying a very strong allowed transition. The γ-ray branch, if any, must be very small since no transitions of the appropriate energies were observed.

The picture of the ^{14}Be β decay that emerges from the present work is in rather good agreement with the shell-model calculation of Curtin and Brown [5]. The principal branch is presumably to a 1^+ state at an excitation energy of 0.97–1.80 MeV in ^{14}B (rather than at 0.94 MeV as in the calculation of Ref. [5]) and with a logft (3.6–3.8) that is consistent with the predicted value of 3.8. Either of the two neutron groups would correspond to a predicted [5] 1^+ state at 4.69 MeV, with branching ratio of 0.5% and logft value 5.5. There is a slightly higher degree of splitting of the main β decay strength in the experimental data, but this is not unexpected given the need for reduction of the basis set in practical shell-model calculations. It remains to observe directly the neutron decay of the low-lying 1^+ state that is just above the $1n$ emission threshold. It would also be of considerable interest to clarify the decays to states above 5 MeV in ^{14}B. Data from n-n and γ-n coincidence experiments would be particularly helpful in this regard.

ACKNOWLEDGMENTS

The authors would like to thank the entire staff of the NSCL for their assistance during this experiment. We also want to thank J. Yurkon for his advice in running the program KSUEFF, K. W. Scheller for his help in the analysis and the use of his data, and, lastly, N. Aoi for valuable comments regarding this work. This work was supported in part by the National Science Foundation, Grant No. PHY 91-00688.

[1] I. Tanihata *et al.*, Phys. Lett. **206B**, 592 (1985).
[2] M. Zahar *et al.*, Phys. Rev. C **48**, R1884 (1993).
[3] F. Ajzenberg-Selove, Nucl. Phys. **A523**, 1 (1991).
[4] J. P. Dufour *et al.*, Phys. Lett. B **206**, 195 (1988).
[5] M. S. Curtin, Ph.D. thesis, Michigan State University, 1985 (unpublished); B. A. Brown (private communication).
[6] B. M. Sherrill, D. J. Morrissey, J. A. Nolen Jr., and J. A. Winger, Nucl. Instrum. Methods Phys. Res. B **56/57**, 1106 (1991).
[7] J. P. Dufour *et al.*, Nucl. Instrum. Methods Phys. Res. A **248**, 267 (1986).
[8] R. Harkewicz *et al.*, Phys. Rev. C **44**, 2365 (1991); R. Harkewicz, Ph.D. thesis, Michigan State University, 1992 (unpublished).
[9] F. Ajzenberg-Selove, Nucl. Phys. **A375**, 1 (1982).
[10] L. Pages, E. Bertel, H. Joffre, and L. Sklavenitis, At. Data **4**, 1 (1972).
[11] F. Ajzenberg-Selove, Nucl. Phys. **A490**, 1 (1988).
[12] D. R. Tilley, H. R. Weller, and H. H. Hasan, Nucl. Phys. **A474**, 1 (1987).
[13] K. W. Scheller *et al.*, Phys. Rev. C **49**, 46 (1994); K. W. Scheller, Ph.D. thesis, University of Notre Dame, 1993 (unpublished).
[14] R. A. Cecil, B. D. Anderson, and R. Madey, Nucl. Instrum. Methods **161**, 439 (1979).
[15] R. J. Kurz, Lawrence Radiation Laboratory Report No. UCRL-11339, 1964 (unpublished).
[16] S. Dixit, program FITS, University of Notre Dame, 1989 (unpublished).
[17] D. J. Morrissey (unpublished).
[18] F. Ajzenberg-Selove, Nucl. Phys. **A506**, 1 (1990).
[19] National Institute of Standards and Technology Certificate of Standard Reference Material, SRM 4275C-69.
[20] L. Wielopolski, Nucl. Instrum. Methods **143**, 577 (1977).
[21] R. Singh, Nucl. Instrum. Methods **136**, 543 (1976).
[22] D. H. Wilkinson and B. E. F. Macefield, Nucl. Phys. **A232**, 58 (1974).
[23] G. Audi and A. H. Wapstra, Nucl. Phys. **A565**, 1 (1993).